DTU Library

Machine learning technique for low-frequency modulation techniques in power converters

Moeini, Amirhossein; Dabbaghjamanesh, Morteza; Dragičević, Tomislav; Kimball, Jonathan W.; Zhang, Jie

Published in:
Control of Power Electronic Converters and Systems

Link to article, DOI:
10.1016/B978-0-12-819432-4.00009-3

Publication date:
2021

Document Version
Publisher's PDF, also known as Version of record

Chapter 6

Machine learning technique for low-frequency modulation techniques in power converters

Amirhossein Moeini[1], Morteza Dabbaghjamanesh[2], Tomislav Dragičević[3], Jonathan W. Kimball[1], Jie Zhang[2]

[1]*Electrical and Computer Engineering Department, Missouri University of Science and Technology, Rolla, MO, United States;* [2]*Department of Mechanical Engineering, The University of Texas at Dallas, Richardson, TX, United States;* [3]*Department of Electrical Engineering, Technical University of Denmark, Lyngby, Denmark*

6.1 Introduction

Nowadays power systems have many new challenges due to the fast growth of electric vehicle charging stations, renewable energy sources, smart grid technologies, and other power electronic−based loads [1−8]. Active power filters (APFs) have been used more and more for compensating the harmonics of nonlinear loads in power systems at the point of common coupling (PCC) [9]. Moreover, both reactive and active power of the power grid at the PCC can be managed by using an APF [9]. Different AC−DC converters have been proposed in the literature for APF applications. Between all available topology, for high-power applications, multilevel converters are growing in popularity due to their low stress on the semiconductor switches, low total harmonic distortion, and modular structure [10,11].

Based on the switching frequency of the converter, the modulation techniques of multilevel converters can be categorized. High-switching frequency modulation techniques such as space vector modulation (SVM) and phase shift−pulse width modulation (PS-PWM) are commonly used due to real-time control on the fundamental and harmonics of the converter and their simple implementation [12]. However, the switching losses of the high-switching frequency modulation techniques are high and undesirable. Moreover, the base-band and side-band harmonics of high-switching frequency modulation techniques are uncontrollable, which are undesirable for the power quality

Control of Power Electronic Converters and Systems. https://doi.org/10.1016/B978-0-12-819432-4.00009-3

requirements of grid-tied converters. On the other hand, low-frequency modulation techniques, e.g., selective harmonic elimination-PWM (SHE-PWM) [13,14], selective harmonic mitigation-PWM (SHM-PWM) [15,16], and selective harmonic current mitigation-PWM (SHCM-PWM) [9,10,17−19], have low switching losses. Contrarily, implementation of these techniques requires huge memory storage to save all possible solutions. By solving transcendental (trigonometric) Fourier series equations, these offline solutions are often obtained.

Different techniques (such as mathematical approaches and linearization techniques) have been proposed in the literature to implement the low-frequency modulation techniques in real time [20]. Contrarily, they are difficult to be implemented for a high-switching frequency. For example, in Ref. [20], an approach was proposed to linearize the trigonometric equations of a low-frequency modulation technique to control harmonic phases and magnitudes of a cascaded H-bridge (CHB) converter. However, the number of harmonics that can be controlled by using [20] is limited.

Artificial intelligence, especially machine learning, has become popular in different applications such as health science, meteorology, military, and education [21]. Machine learning can be used for regression or classification by using different training techniques [21]. One of the most commonly used machine learning techniques is artificial neural network (ANN) [22−30]. In ANN, the learning behavior of the human brain is modeled by using mathematical equations. The ANN has also been used for the grid-tied converter low-frequency modulation technique in Refs. [22,31], to utilize the DC-link voltages of the grid-tied converter for controlling the switching angles of the SHE-PWM. Contrarily, existing work in the literature have not extensively investigated how to apply ANN for a real-time implementation of the low-frequency modulation technique with a high number of switching transitions, how to generate training dataset, or how to control both magnitudes and phases of the voltage harmonics of grid-tied converters for the APF application.

As discussed in Ref. [9], the quarter-wave symmetric modulation techniques such as SHE-PWM, SHCM-PWM, and SHM-PWM cannot control both magnitude and phase of the voltage harmonic of the grid-tied converters. To solve this issue, when the low-frequency modulation technique is applied for the grid-tied converter, a half-wave symmetric modulation technique, e.g., asymmetric selective harmonic current mitigation-PWM (ASHCM-PWM) [18] can be used as discussed in Ref. [9]. As a result, when the low-frequency modulation technique is applied for the grid-tied converter, the ASHCM-PWM is the only option for controlling the APF current harmonics. The proposed technique has not been investigated so far by using ASHCM-PWM technique for the grid-tied converter. In this chapter, an asymmetric selective harmonic current mitigation-PWM (ASHCM-PWM) real-time implementation is investigated by using the ANN technique. As it will be shown in this chapter, the conventional lookup tables can be replaced by a trained ANN for controlling harmonics and the fundamental of the APF. Furthermore, when nonlinear loads are connected at the PCC, the current harmonic requirements of the IEEE Std. 519 [32] can be met by using the proposed technique at the PCC. To reach this goal, a 3-cell 7-level CHB grid-tied converter is employed in both simulations and experiments of this chapter.

The remaining of this chapter is organized as follows. Section 6.2 briefly discusses the APFs fundamental principles. Section 6.3 explains the proposed ANN technique for the low-frequency modulation technique. The proposed ANN technique simulation and experimental results are shown and discussed in Section 6.4. Finally, Section 6.5 concludes the work.

6.2 Cascaded H-bridge active power filter configuration

Fig. 6.1 shows a CHB converter configuration for the APF application. As shown in Fig. 6.1, the CHB converter N cells are connected to the grid by using the coupling inductance (L_F). The nonlinear loads are also connected to the PCC and inject the nonlinear load current ($i(_{NLL})$). The converter generates the current ($i(_{ac-CHB})$) as shown in Fig. 6.1 to compensate for the nonlinear load current. By applying KCL,

$$i_{in}(t) = i_{(ac-CHB)}(t) + i_{(NLL)}(t). \tag{6.1}$$

where i_{in} is the injected current to the power grid. R_{grid} and L_{grid} are the resistance and inductance of the power grid, respectively. In this chapter, the power grid parameters are ignored. $v(_{ac-Grid})(t)$, $v(_{ac-CHB})(t)$, and $v(_{pcc})(t)$ are the AC voltages of the grid, CHB, and PCC in Fig. 6.1, respectively.

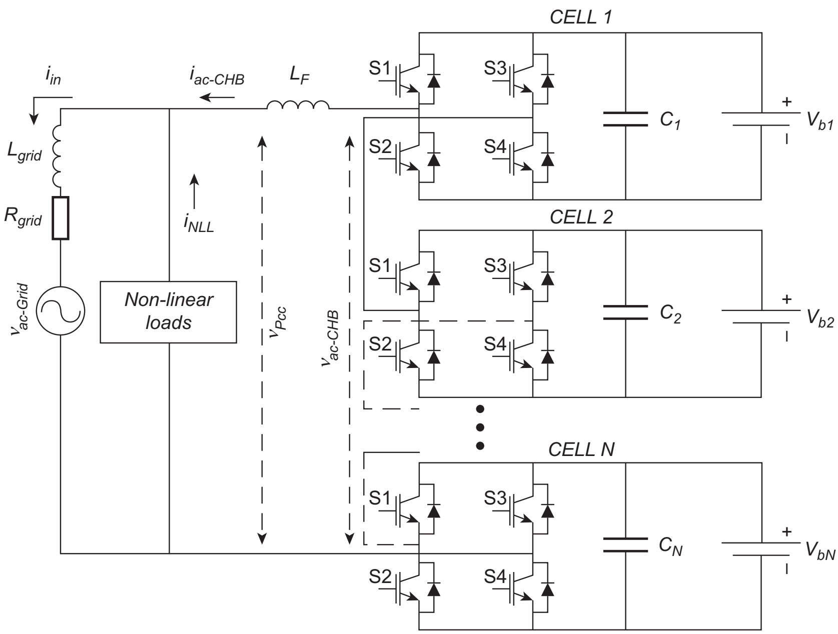

FIGURE 6.1 Configuration of the CHB for APF application.

6.3 ANN for the asymmetric selective harmonic current mitigation-PWM

One of the key challenges in low-frequency modulation techniques is to find real-time solutions of the Fourier equations for different phases and magnitudes of fundamental and harmonics. The proposed ANN-based technique can be used to reach this goal. The CHB voltage Fourier series equations in Fig. 6.2, with half-wave symmetry for the CHB voltage, is

$$\begin{cases} v_{(ac-CHB)}(t) = \sum_{h=1}^{\infty}\left(a_h\cos(h\omega t) + b_h\sin(h\omega t)\right) \\ a_h = \dfrac{2V_{dc}}{h\pi}\begin{pmatrix} -\sin(h\theta_{11}) + \sin(h\theta_{12}) - \cdots - \sin(h\theta_{in1}) \\ +\sin(h\theta_{i(n_i+1)}) - \cdots + \sin(h\theta_{1(2n1)}) \end{pmatrix} \\ b_h = \dfrac{2V_{dc}}{h\pi}\begin{pmatrix} \cos(h\theta_{11}) - \cos(h\theta_{12}) + \cdots + \cos(h\theta_{ini}) \\ -\cos(h\theta_{i(n_i+1)}) + \cdots - \cos(h\theta_{1(2n1)}) \end{pmatrix} \\ 0 \le \theta_{11} \le \theta_{12} \le \cdots \\ \ldots \le \theta_{in_i} \le \theta_{i(n_i+1)} \le \ldots\theta_{1(2n_1)} \le \pi \end{cases} \tag{6.2}$$

where b_h and a_h are the h_{th} order sine and cosine components of the CHB voltage, respectively; V_{dc} is the DC-link voltage of the converter ($V_{dc} = V_{b1} = V_{b2} = \ldots = V_{bN}$); θ_{jk} is the jth cell kth switching transition of the converter. The KVL equation of Fig. 6.1, when the effects of the impedance of the grid and the resistance of L_F are ignored, is written as

$$v_{(ac-CHB)}(t) = v_{(pcc)}(t) + L_F\frac{di_{(ac-CHB)}}{dt}. \tag{6.3}$$

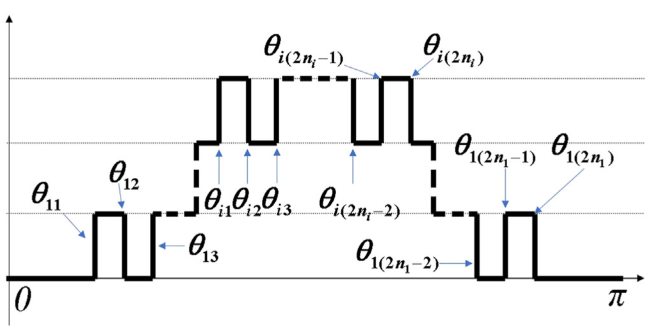

FIGURE 6.2 The time-domain waveform of the active power filter generating the voltage $v_{(ac-CHB)}(t)$.

TABLE 6.1 Odd order current harmonic requirements of the IEEE Std. 519 [32].

Harmonic order	Current limit (%)
$1 < h < 11$	4
$11 < h < 17$	2
$17 \leq h < 23$	1.5
$23 \leq h < 35$	0.6
$35 \leq h < 50$	0.3
TDD	5

The IEEE Std. 519 [32] requirements are then used to impose restrictions on the frequency-domain components of I_{in}. In ASHCM-PWM, where C_h is the hth order current harmonic requirement of IEEE Std. 519 [32] as shown in Table 6.1, the hard equalities of SHE-PWM are replaced by inequalities given in (6.4), when $\frac{I_L}{I_{sc}} \leq 20$. I_L is the maximum demand load at the PCC. I_{sc} is the converter short circuit current at the PCC. K is the switching transitions total number of the ASHCM-PWM.

In order to meet the current harmonic requirements, the ASHCM-PWM technique must generate the CHB voltage. In conventional approaches, off-line solutions of (6.4) are obtained for a wide range of phases and magnitudes for the harmonics and fundamental, which requires an impractically large memory for embedded implementation. In the present work, an ANN structure is used instead. In order to meet the current harmonic requirements listed in Table 6.1, the injected current harmonic $I_{ac-CHB-h}$ should have equal magnitude as, and 180 degrees phase shift from, I_{NLL-h}. When the magnitude is changed from 0 to $|I_{NLL-h}|$ and the phase is changed from 0 to 360 degrees, a low number of switching angles in the ASHCM-PWM technique cannot mitigate the h_{th} nonlinear load current harmonic. Therefore, the maximum circle whole range of nonlinear load current harmonics can be divided into several sections (24 sections in Fig. 6.3). This helps to have all solutions that are close to each other in a same section of Fig. 6.3. This helps the proposed learning-based technique to better divide all solutions (training data) based on the section into which each order of harmonics is placed.

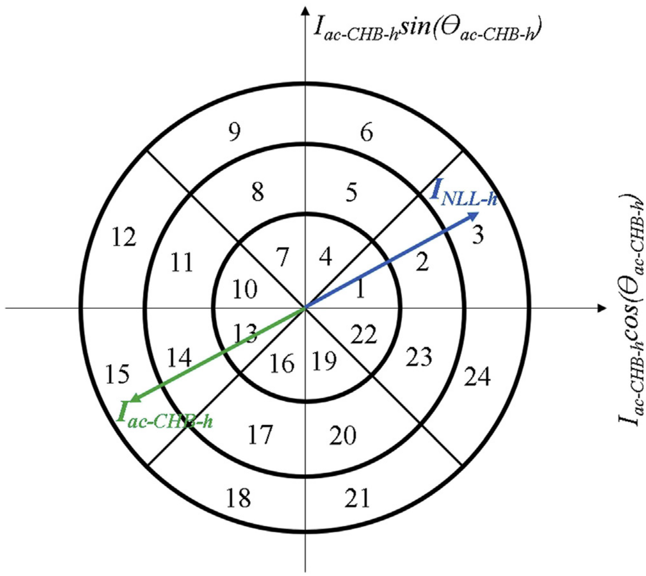

FIGURE 6.3 The proposed ANN technique for controlling current harmonics of APF.

$$
\begin{cases}
a_1 = \dfrac{2V_{dc}}{\pi}\left(-\sin(\theta_{11}) + \sin(\theta_{12}) - \ldots + \sin(\theta_K)\right), \\
b_1 = \dfrac{2V_{dc}}{\pi}\left(\cos(\theta_{11}) - \cos(\theta_{12}) + \ldots - \cos(\theta_K)\right), \\
\left| \dfrac{b_1 + ja_1 - V_{(pcc-1)}\left(\cos\left(\angle V_{(pcc-1)}\right) + j\sin\left(\angle V_{(pcc-1)}\right)\right)}{j\omega L_F} \begin{matrix} \ldots + I_{(NLL-1)}\left(\cos\left(\angle I_{(NLL-1)}\right) + j\sin\left(\angle I_{(NLL-1)}\right)\right) \\ \ldots - I_{(in-1)}\left(\cos\left(\angle I_{(in-1)}\right) + j\sin\left(\angle I_{(in-1)}\right)\right) \end{matrix} \right| \leq \varepsilon_1, \\
\left|\dfrac{I_{(in-3)}}{I_L}\right| = \left| \dfrac{b_3 + ja_3 - V_{(pcc-3)}\left(\cos\left(\angle V_{(pcc-3)}\right) + j\sin\left(\angle V_{(pcc-3)}\right)\right)}{(j3\omega L_F I_L)} \ldots + I_{NLL-3}\left(\cos\theta_{NLL-3} + j\sin\theta_{NLL-3}\right) \right| \leq C_3, \\
\left|\dfrac{I_{(in-5)}}{I_L}\right| = \left| \dfrac{b_5 + ja_5 - V_{(pcc-5)}\left(\cos\left(\angle V_{(pcc-5)}\right) + j\sin\left(\angle V_{(pcc-5)}\right)\right)}{(j5\omega L_F I_L)} \ldots + I_{NLL-5}\left(\cos\theta_{NLL-5} + j\sin\theta_{NLL-5}\right) \right| \leq C_5, \\
\left|\dfrac{I_{(in-h)}}{I_L}\right| = \left| \dfrac{b_h + ja_h - V_{(pcc-h)}\left(\cos\left(\angle V_{(pcc-h)}\right) + j\sin\left(\angle V_{(pcc-h)}\right)\right)}{(jh\omega L_F I_L)} \ldots + I_{NLL-h}\left(\cos\theta_{NLL-h} + j\sin\theta_{NLL-h}\right) \right| \leq C_h,
\end{cases}
\tag{6.4}
$$

In Fig. 6.3, there are 24 sections for different magnitudes and phases of I_{NLL-h}. Using a high number of sections can improve the ANN performance to meet the power quality standards in the ASHCM-PWM technique. Contrarily, this can also significantly increase the size of the dataset. Thus, the proposed technique computational burden is significantly increased. In this technique, the total demand distortion (TDD) is not controlled and just the current harmonics are controlled, given by

$$\mathrm{TDD} = \sqrt{\left(\frac{I_{in-3}}{I_L}\right)^2 + \left(\frac{I_{in-5}}{I_L}\right)^2 + \cdots + \left(\frac{I_{in-h}}{I_L}\right)^2} \tag{6.5}$$

However, controlling the individual harmonics will generally achieve the desired TDD as well.

In Fig. 6.3, the $I_{ac-CHB-h}$ can be determined as

$$\begin{cases} I_{(ac-CHB-1)} = \dfrac{b_1 + ja_1 - V_{(pcc-1)}\left(\cos\left(\angle V_{(pcc-1)}\right) + j\sin\left(\angle V_{(pcc-1)}\right)\right)}{(j\omega L_F)}, \\ I_{(ac-CHB-3)} = \dfrac{b_3 + ja_3 - V_{(pcc-3)}\left(\cos\left(\angle V_{(pcc-3)}\right) + j\sin\left(\angle V_{(pcc-3)}\right)\right)}{(j3\omega L_F)}, \\ I_{(ac-CHB-5)} = \dfrac{b_5 + ja_5 - V_{(pcc-5)}\left(\cos\left(\angle V_{(pcc-5)}\right) + j\sin\left(\angle V_{(pcc-5)}\right)\right)}{(j5\omega L_F)} \\ \cdots \\ I_{(ac-CHB-h)} = \dfrac{b_h + ja_h - V_{(pcc-h)}\left(\cos\left(\angle V_{(pcc-h)}\right) + j\sin\left(\angle V_{(pcc-h)}\right)\right)}{(jh\omega L_F)} \end{cases} \tag{6.6}$$

The solutions of (6.6) are solved for various phases and magnitudes of V_{PCC-h}. By checking the phase and magnitude of (6.6), one of the sectors in Fig. 6.3 is selected. In this paper, it is assumed that the PCC voltage harmonic magnitudes are close to zero. Contrarily, the PCC voltage harmonics can be obtained from

$$V_{(PCC)}(s) = \frac{sL_F V_{(ac-Grid)}(s) + Z_{Grid}(s)\left(V_{(ac-CHB)}(s) + sL_F I_{NLL}(s)\right)}{\left(sL_F + Z_{Grid}(s)\right)}, \tag{6.7}$$

where $Z_{Grid}(s)$ is the grid impedance. From (6.7), a high value of $Z_{Grid}(s)$ increases the $V(_{ac-CHB})$ effect on the V_{PCC}. However, a low value of $Z_{Grid}(s)$ increases the effect of $V(_{ac-Grid})(s)$ on the $V_{PCC}(s)$. From (6.6) and (6.7), $I(_{ac-CHB})$ is a function of $V(_{ac-CHB})$ and V_{PCC}. Furthermore, V_{PCC} is also function of $V(_{ac-CHB})$. Thus, changing the $V(_{ac-CHB})$ affects both V_{PCC}

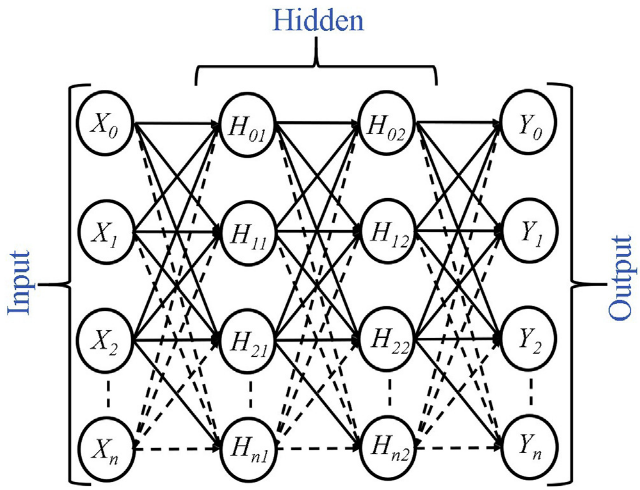

FIGURE 6.4 The ANN block diagram to be applied in the active power filter.

and $I(_{ac-CHB})$. This can complicate the controller design when the grid has an impedance, and is beyond the scope of the present work. Eq. (6.6) data for various switching angles of the CHB converter are obtained.

A general block diagram of the ANN [21] is shown in Fig. 6.4. As it can be seen, three main layers are used for the ANN technique: an input layer (X), an output layer (Y), and two hidden layers (H). Several nodes are used as shown in Fig. 6.4. Among consecutive layers (i (previous layer) and j (current layer)), a line which has a weight (ω_{ij}) is used. Each node output can be calculated using

$$O_j^l = \sigma_j^l\left(\sum_{i=0}^{n_{l-1}}\left(O_i^{l-1}\omega_{ij}\right) + b_j^l\right) \tag{6.8}$$

where O_j^l is the output of the lth layer jth node, O_j^{l-1} is the output of the $(l-1)$ th layer jth node, O_j^l is the jth node activation function in the lth layer, b_j^l is the bias of the jth node in the lth layer of the ANN, and n_{l-1} is the number of nodes in the $(l-1)$th layer.

In the proposed method, values of θ_{11}, θ_{12}, …, and θ_K that satisfy (6.4) are determined for a PCC voltage harmonic magnitudes and phases range. Given the large number of variables and the range of inputs, the search space is very large. Thus, the technique given in Algorithm 6.1 is used to randomly sample the search space.

Algorithm 6.1 is used to generate random training data. First, based on the accuracy that is required for the harmonics and the available computational power, a time step is chosen. Switching angles that cover the whole range of search space are produced using random numbers. For the present work, the time step is set to 8 degrees; a smaller time step corresponds to an increase in the dataset size, an increase in the time required for training, and an increase in accuracy. The proposed algorithm first sorts the angles produced. Next, the angles are checked to all lie within the range of [0 degree; 180 degrees] to enforce half-wave symmetry. By using (6.4) and the obtained switching angles, current harmonics are checked to determine whether they meet the IEEE Std. 519 limits [32]. Variables O_3, O_5, …, O_h, O_{TDD} are logical indicators of whether the results satisfy the given limits; additional constraints can be included for other power quality standards. Finally, O_1 assigns the fundamental voltage (b_1).

6.4 The proposed technique simulation and experimental results

To validate the advantages and effectiveness of the proposed ASHCM-PWM with the ANN technique, simulation and experimental results are obtained for a 3-cell 7-level CHB converter. The parameters (i.e., the circuit parameters and the number of hidden layers of the ANN) of the grid-tied converter during the simulations and experiments are shown in Tables 6.2 and 6.3. The open-source KERAS [33] software is used to train the ANN, which is written in Python. The main objective in both simulations and experiments is to prove that the ANN technique can control harmonic phases and magnitudes by using the ASHCM-PWM technique.

6.4.1 Simulation results

In addition to the parameters that are mentioned in Table 6.2, a diode bridge connected to a parallel combination of a 20 resistor and a 50 μF capacitor is

TABLE 6.2 The number of nodes in ANN hidden layers.

Technique	1st hid.	2nd hid.	3rd hid.	4th hid.
ANN	50	50	50	50

TABLE 6.3 Multilevel converter parameters in simulations and experiments.

Parameter	Symbol	Value
AC grid voltage	$V_{ac-Grid-1}$	110 V
Fundamental frequency	F	60 Hz
Coupling inductance	L_F	0.49 pu
DC-link voltage	V_{dc}	65 V
Maximum output demand current	I_L	20 A
Number of cells in CHB	i	3
Number of switching transitions in each cell	n	1
Number of switching transitions	K	3
Number of mitigated harmonics	h	49
Decoupling DC capacitance	C	600 µF

used as a nonlinear load in the first simulation. Grid impedance is neglected here so the rectifier does not affect the PCC voltage. MATLAB/Simulink[1] is used to simulate the nonlinear load combination and the CHB grid-tied converter. Fig. 6.5A illustrates the time-domain waveforms of $i_{in}(t)$, $v_{(ac-CHB)}(t)$, $v_{(ac-Grid)}(t)$, and $i_{NLL}(t)$. The ANN technique increases the $i_{in}(t)$ fundamental current from 7:77 to 19:2 A at the PCC. Fig. 6.5B shows the current harmonic spectra of the nonlinear load ($i_{NLL}(t)$), which cannot meet the current harmonic requirements (the red (gray in print version) line in Fig. 6.5B) of the IEEE Std. 519 [32] for the third and fifth harmonics. Moreover, the nonlinear load current TDD cannot meet the 5% limit of the IEEE Std. 519. Fig. 6.5C shows the current harmonic spectra of $i_{in}(t)$ at the PCC, when the nonlinear load ($i_{NLL}(t)$) is injected to the grid. Now, the harmonics do meet the requirements due to the compensation provided by the CHB. The ANN achieves harmonic control with only six switching transitions per half-period.

1. MATLAB and Simulink are registered trademarks of The MathWorks, Inc.

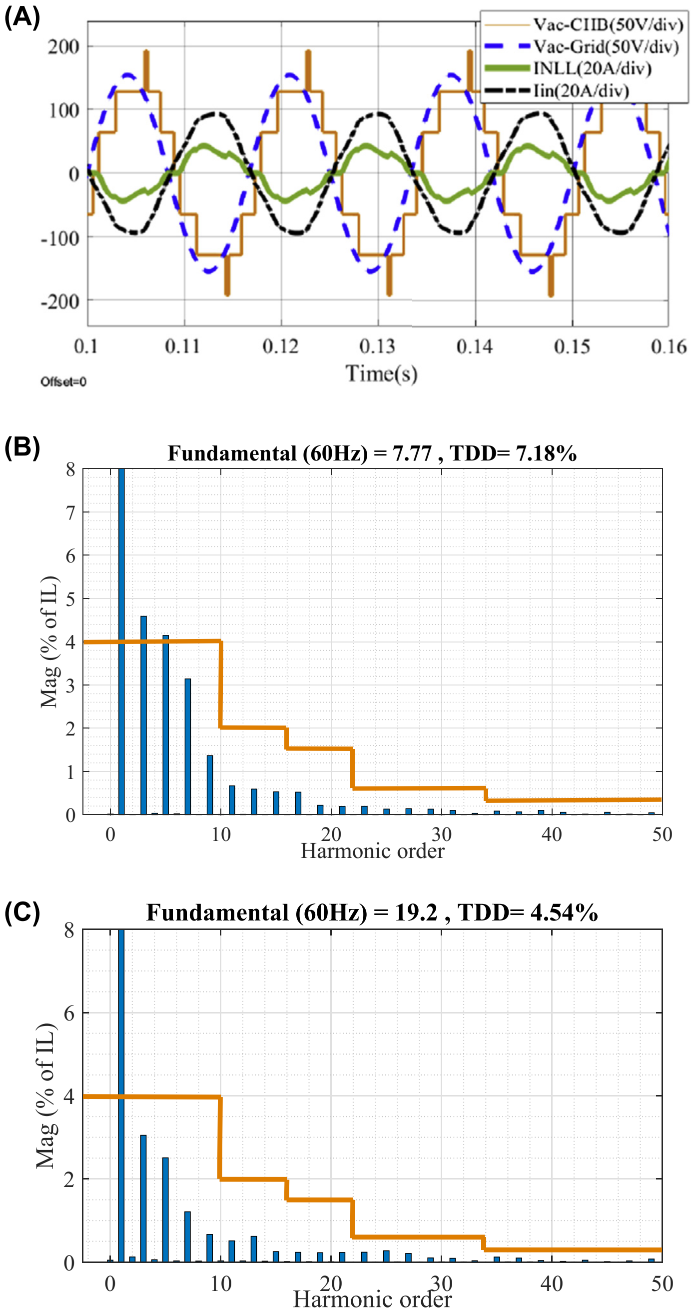

FIGURE 6.5 Simulation results using ASHCM-PWM technique for the grid-tied CHB converter with a nonlinear load, (A) time-domain waveforms of the $v(_{ac-CHB})(t)$, $v(_{ac-Grid})(t)$, $i_{in}(t)$, and $i(_{NLL})(t)$; (B) current harmonic spectra of $i(_{NLL})(t)$; (C) current harmonic spectra of $i_{in}(t)$.

Algorithm 6.1. (*The proposed ASHCM-PWM algorithm with ANN.*)

Algorithm 1 The proposed ASHCM-PWM algorithm with ANN

```
for sw_11 = 1, 8, 16, ..., 180 − 8k do
    for sw_12 = sw_11, sw_11 + 8, sw_11 + 16, ..., 172 − 8k do
        ...
        for sw_in_i = sw_in_{i−1}, sw_in_i = sw_in_{i−1} + 8, sw_in_i = sw_in_{i−1} + 16, ..., sw_in_i = 180 do
            θ_11 = 8 * random number + sw_11
            ...
            θ_in_i = 8 * random number + sw_in_i
            sort(θ_11, θ_12, ..., θ_in_i)
            for j=1:number of cells of converter do
                for p=1:number of switching in jth cell do
                    if θ_jp ≤ 180° then
                        θ_jp = 180°
                    end
                end
            end
            if (|I_{in−3} / I_L| ≤ C_3) then
                O_3=1
            else
                O_3=0
            end
            ...
            if (|I_{in−h} / I_L| ≤ C_h) then
                O_h=1
            else
                O_h=0
            end
            if (|TDD| > 5%) then
                O_TDD=0
            else
                O_TDD=1
            end
            O_1 = b_1
        end
    end
end
```

Fig. 6.6 shows the ANN technique second simulation result when the modulation index of the converter with the ASHCM-PWM is 2.45. The second simulation result objective is to prove that the ANN can control the current harmonic for the ASHCM-PWM without injecting the nonlinear load to the grid. After training the ANN technique, the proposed technique switching angles are 3, 26, 48, 121, 147, and 165 degrees. The grid-tied converter current magnitude is 12:9 A with a phase of 104 degrees. Thus, the proposed technique can be applied to the grid-tied converter for any reactive and active power. Fig. 6.6A shows the time-domain waveforms of $i_{in}(t)$, $v_{ac-CHB}(t)$, and

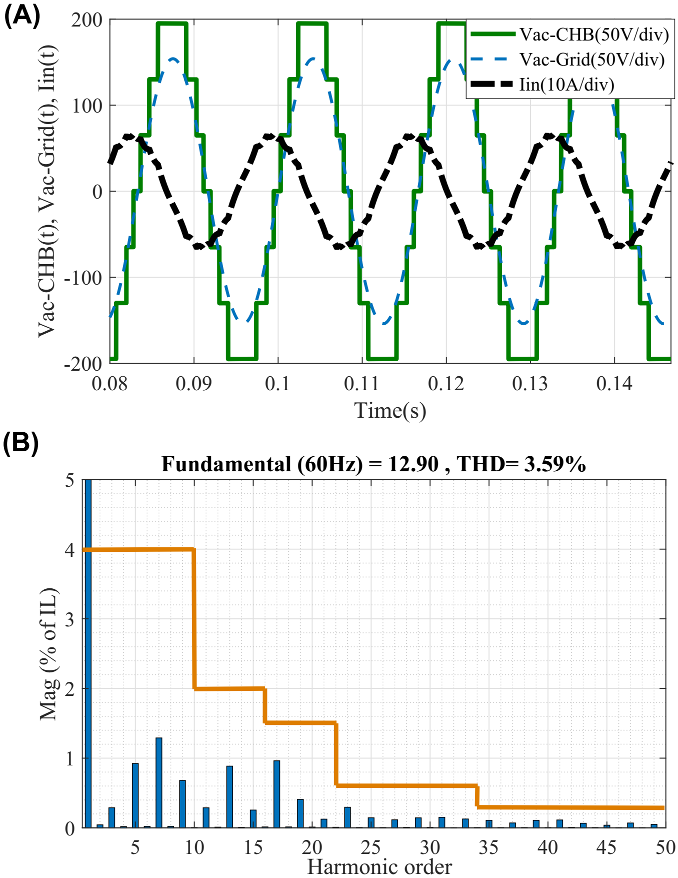

FIGURE 6.6 ASHCM-PWM technique simulation results for the grid-tied CHB converter without the nonlinear load, (A) time-domain waveforms of $v(_{ac-CHB})(t)$, $v(_{ac-Grid})(t)$, and $i_{in}(t)$, (B) current harmonic spectra of $i(_{in})(t)$.

$v_{ac-Grid}(t)$. In this figure, a sinusoidal waveform is generated for the AC current ($i_{in}(t)$) by using the low-frequency modulation technique. Moreover, there is no variation in $v_{ac-CHB}(t)$ time-domain waveform due to neglecting the parasitic resistance at the DC link. On the contrary, the proposed technique can meet the power quality standard, when there is a parasitic resistance at the DC link of the CHB converter (internal resistance of the battery) as proven in Ref. [34]. The AC current time-domain waveform (($i_{in}(t)$)) is shown in Fig. 6.6B with the requirements of the IEEE Std. 519 indicated. From this figure, the proposed ANN can control all 25 odd low-order current harmonics. Also, as shown in Fig. 6.6B, the TDD 5% limit in IEEE Std. 519 can be met by using the ANN.

6.4.2 Experimental results

An ANN technique is further validated with experimental results using the same parameters, a 3-cell 7-level CHB converter. The second simulation in Fig. 6.6 is experimentally repeated using the same parameters. The grid-tied CHB converter hardware prototype that is used in experiments is shown in Fig. 6.7. Texas Instruments TMS320F28335 is used for applying the switching angles to the CHB converter. In each H-bridge of the CHB converter, an intelligent power module (IPM) (rated 30 A and 600 V) that uses a 3-leg IGBT is used as shown in Fig. 6.7. The block diagram in Fig. 6.8 illustrates the proposed technique implementation during the experiments, which is an open-loop control that applies the ASHCM-PWM switching angles technique with the ANN. The grid impedance is small and may be ignored as shown in Fig. 6.8. A phase-locked loop is used in this figure to detect the phase and frequency of the grid voltage. Moreover, θ_{CHB} is the CHB converter initial phase. In both simulation and experimental results,

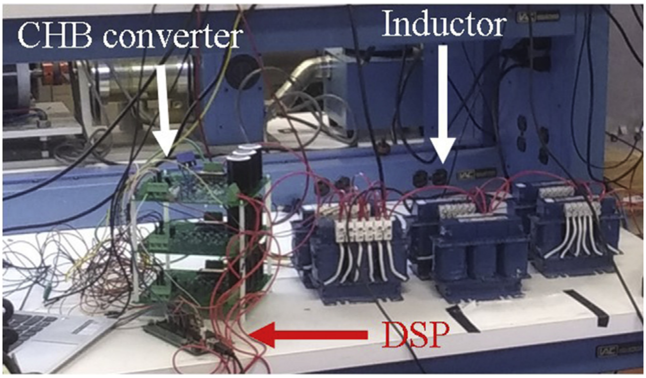

FIGURE 6.7 3-cell grid-tied CHB converter hardware prototype.

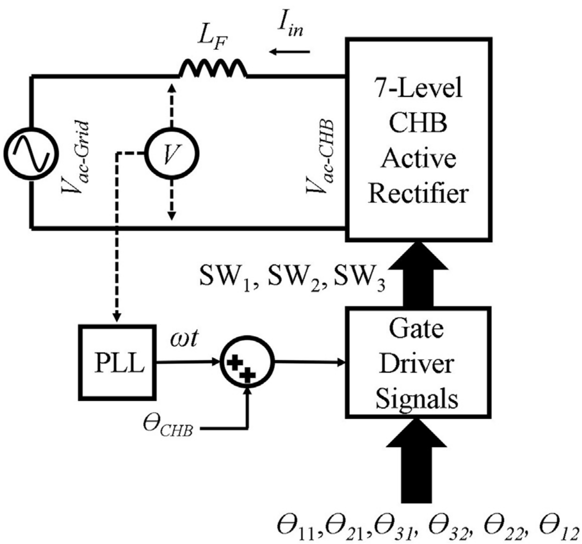

FIGURE 6.8 Grid-tied converter block diagram during the experiments and simulations.

the θ_{CHB} is assumed to be 0 degree. The optimal solutions (switching angles) (θ_{11}, θ_{21}, θ_{31}, θ_{32}, θ_{22}, θ_{12}) in Fig. 6.8 from the ANN are used in the grid-tied CHB converter. The switching transition values that are employed in the experiment are the same as in the second simulation result shown in Fig. 6.6. SW_1; SW_2; and; SW_3 are the converter switchings for the first, second, and third H-bridge cells, respectively. The converter has the lowest possible switching frequency, equal to the line frequency, 60 Hz. As a result, the proposed technique has the lowest possible switching losses for hard switching AC−DC converters.

The experimental results of the proposed ANN technique for ASHCM-PWM are shown in Fig. 6.9, when the CHB converter modulation index is 2.45, the same as the simulation result in Fig. 6.6. The grid-tied converter AC current is 13:4 A with a phase of 102. The $v_{ac-CHB}(t)$, $v_{ac-Grid}(t)$, and $i_{in}(t)$ time-domain waveforms are shown in Fig. 6.9A. The AC input current ($i_{in}(t)$) has a pure sinusoidal current waveform similar to the simulation result. The experimental current harmonic spectrum is shown in Fig. 6.9B. The IEEE Std. 519 [32] current requirements are shown by the red (gray in print version) line in Fig. 6.9B. As illustrated in the experimental results, all low-order current harmonics meet the IEEE Std. 519 requirements at the PCC. Moreover, using the proposed ANN technique for the ASHCM-PWM in the experiment in Fig. 6.9B, the 5% limit specified in the IEEE Std. 519 for the TDD is met.

(A)

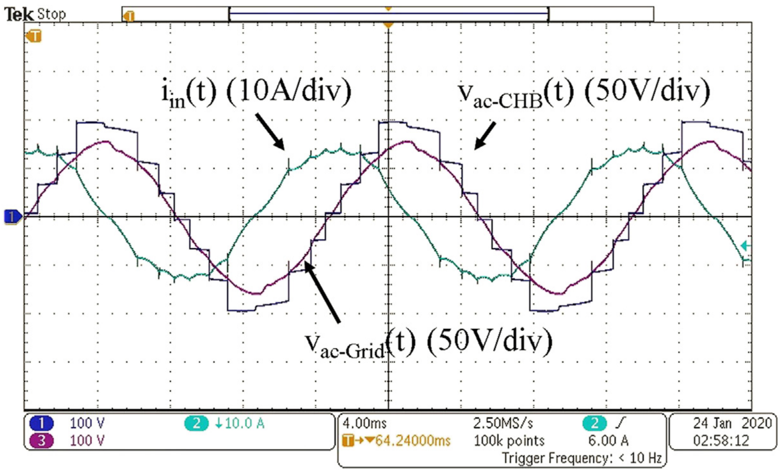

(B)

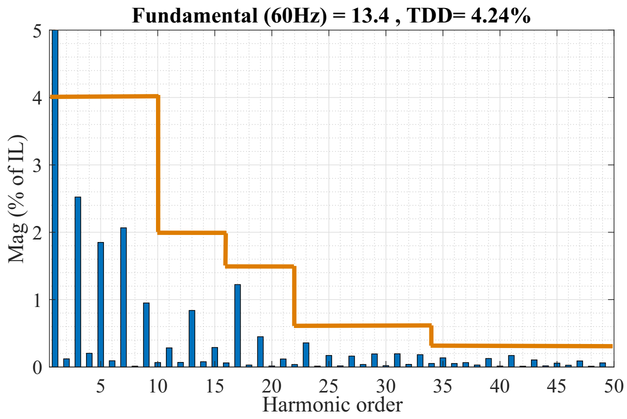

FIGURE 6.9 ASHCM-PWM technique experimental results for the grid-tied CHB converter, (A) time-domain waveforms of $v(_{ac-CHB})(t)$, $v(_{ac-Grid})(t)$, and $i_{in}(t)$, (B) current harmonic spectra of $i(_{in})(t)$.

6.5 Conclusion

In this chapter, an ANN technique to implement asymmetric selective harmonic current mitigation-PWM was proposed to control the current harmonics at the PCC in order to meet the power quality standards. The proposed technique does not need to save all phases and magnitudes of the fundamental and harmonics of the APF application AC current. The low-frequency ASHCM-PWM technique was implemented in both simulations and experiments to prove the advantages of the proposed technique for controlling the APF current harmonic. To reach this goal, a technique was proposed to categorize the voltage harmonic vectors of the grid-tied converter. As demonstrated in the simulation and experimental results, the proposed technique that uses an ANN could meet the power quality standard low-order current harmonics such as the IEEE Std. 519. Furthermore, in this chapter, a guideline for generating the ANN technique training data was proposed. Using the guidelines in this chapter, the ANN could completely search the solutions whole search space of the low-frequency modulation techniques.

References

[1] M. Dabbaghjamanesh, A. Kavousi-Fard, Z. Dong, A novel distributed cloud-fog based framework for energy management of networked microgrids, IEEE Trans. Power Syst. 35 (4) (2020) 2847−2862.

[2] M. Dabbaghjamanesh, A. Kavousi-Fard, S. Mehraeen, J. Zhang, Z.Y. Dong, Sensitivity analysis of renewable energy integration on stochastic energy management of automated reconfigurable hybrid ac−dc microgrid considering DLR security constraint, IEEE Trans. Industr. Inform. 16 (1) (January 2020) 120−131.

[3] M. Dabbaghjamanesh, B. Wang, A. Kavousi-Fard, S. Mehraeen, N.D. Hatziargyriou, D. Trakas, F. Ferdowsi, A novel two-stage multi-layer constrained spectral clustering strategy for intentional islanding of power grids, IEEE Trans. Power Deliv. 35 (2) (2019) 560−570.

[4] M. Dabbaghjamanesh, A. Kavousi-Fard, S. Mehraeen, Effective scheduling of reconfigurable microgrids with dynamic thermal line rating, IEEE Trans. Ind. Electron. 66 (2) (February 2019) 1552−1564.

[5] E. Taherzadeh, M. Dabbaghjamanesh, M. Gitizadeh, A. Rahideh, A new efficient fuel optimization in blended charge depletion/charge sustenance control strategy for plug-in hybrid electric vehicles, IEEE Trans. Intell. Veh. 3 (3) (September 2018) 374−383.

[6] M. Dabbaghjamanesh, B. Wang, S. Mehraeen, J. Zhang, A. Kavousi-Fard, Networked microgrid security and privacy enhancement by the blockchain-enabled internet of things approach, in: 2019 IEEE Green Technologies Conference (GreenTech), April 2019, pp. 1−5.

[7] A. Kavousi Fard, B. Wang, O. Avatefipour, M. Dabbaghjamanesh, R. Sahba, A. Sahba, Superconducting fault current limiter allocation in reconfigurable smart grids, in: 2019 3rd International Conference on Smart Grid and Smart Cities (ICSGSC), June 2019, pp. 76−80.

[8] M. Dabbaghjamanesh, S. Mehraeen, A. Kavousi-Fard, F. Ferdowsi, A new efficient stochastic energy management technique for interconnected ac microgrids, in: 2018 IEEE Power Energy Society General Meeting (PESGM), August 2018, pp. 1−5.

[9] A. Moeini, S. Wang, An asymmetric selective harmonic current and voltage modulation-PWM technique for electric vehicle charging stations with cascaded h-bridge converters to meet power quality standards, in: 2019 IEEE Energy Conversion Congress and Exposition (ECCE), September 2019, pp. 4395−4402.

[10] A. Moeini, H. Zhao, S. Wang, A current-reference-based selective harmonic current mitigation PWM technique to improve the performance of cascaded h-bridge multilevel active rectifiers, IEEE Trans. Ind. Electron. 65 (1) (2016) 727−737.

[11] A. Moeini, H. Iman-Eini, M. Bakhshizadeh, Selective harmonic mitigation-pulse-width modulation technique with variable dc-link voltages in single and three-phase cascaded h-bridge inverters, IET Power Electron. 7 (4) (2013) 924−932.

[12] M.S.A. Dahidah, G. Konstantinou, V.G. Agelidis, A review of multilevel selective harmonic elimination PWM: formulations, solving algorithms, implementation and applications, IEEE Trans. Power Electron. 30 (8) (August 2015) 4091−4106.

[13] S.R. Pulikanti, V.G. Agelidis, Hybrid flying-capacitor-based active-neutral-point-clamped five-level converter operated with she-PWM, IEEE Trans. Ind. Electron. 58 (10) (October 2011) 4643−4653.

[14] H. Zhao, S. Wang, A. Moeini, Critical parameter design for a cascaded h-bridge with selective harmonic elimination/compensation based on harmonic envelope analysis for single-phase systems, IEEE Trans. Ind. Electron. 66 (4) (April 2019) 2914−2925.

[15] L.G. Franquelo, J. Napoles, R.C.P. Guisado, J.I. Leon, M.A. Aguirre, A flexible selective harmonic mitigation technique to meet grid codes in three-level PWM converters, IEEE Trans. Ind. Electron. 54 (6) (December 2007) 3022−3029.

[16] M. Najjar, A. Moeini, M.K. Bakhshizadeh, F. Blaabjerg, S. Farhangi, Optimal selective harmonic mitigation technique on variable dc link cascaded h-bridge converter to meet power quality standards, IEEE J. Emerging Sel. Top. Power Electron. 4 (3) (September 2016) 1107−1116.

[17] A. Moeini, H. Zhao, S. Wang, Improve control to output dynamic response and extend modulation index range with hybrid selective harmonic current mitigation-PWM and phase-shift PWM for four-quadrant cascaded h-bridge converters, IEEE Trans. Ind. Electron. 64 (9) (2017) 6854−6863.

[18] A. Moeini, S. Wang, B. Zhang, L. Yang, A hybrid phase shift-PWM and asymmetric selective harmonic current mitigation-PWM modulation technique to reduce harmonics and inductance of single-phase grid-tied cascaded multilevel converters, IEEE Trans. Ind. Electron. (2019), 1−1.

[19] A. Moeini, S. Wang, Analyzing and reducing current harmonics of ac and dc sides of cascaded h-bridge converters for electric vehicle charging stations, in: 2019 IEEE Energy Conversion Congress and Exposition (ECCE), September 2019, pp. 193−200.

[20] H. Zhao, T. Jin, S. Wang, L. Sun, A real-time selective harmonic elimination based on a transient-free inner closedloop control for cascaded multilevel inverters, IEEE Trans. Power Electron. 31 (2) (February 2016) 1000−1014.

[21] J.M. Zurada, Introduction to Artificial Neural Systems, vol. 8, West Publishing Company St. Paul, 1992.

[22] F. Filho, L.M. Tolbert, Y. Cao, B. Ozpineci, Real-time selective harmonic minimization for multilevel inverters connected to solar panels using artificial neural network angle generation, IEEE Trans. Ind. Appl. 47 (5) (September 2011) 2117−2124.

[23] M. Balasubramonian, V. Rajamani, Design and real-time implementation of shepwm in single-phase inverter using generalized hopfield neural network, IEEE Trans. Ind. Electron. 61 (11) (November 2014) 6327−6336.

[24] K. Yang, J. Hao, Y. Wang, Switching angles generation for selective harmonic elimination by using artificial neural networks and quasi-newton algorithm, in: 2016 IEEE Energy Conversion Congress and Exposition (ECCE), September 2016, pp. 1−5.

[25] P. Farhadi, M. Navidi, M. Gheydi, M. Pazhoohesh, H. Bevrani, Online selective harmonic minimization for cascaded half-bridge multilevel inverter using artificial neural network, in: 2015 Intl Aegean Conference on Electrical Machines Power Electronics (ACEMP), 2015 Intl Conference on Optimization of Electrical Electronic Equipment (OPTIM) 2015 Intl Symposium on Advanced Electromechanical Motion Systems (ELECTROMOTION), September 2015, pp. 331−335.
[26] P. Shanmuga Aravind, S. Albert Alexander, Harmonic minimization of a solar fed cascaded H bridge inverter using artificial neural network, in: 2013 International Conference on Energy Efficient Technologies for Sustainability, April 2013, pp. 163−167.
[27] I. Khoukha, C. Hachemi, B. El Madjid, Ann control of nine level NPC voltage inverter based on selective harmonics elimination, in: 2007 International Aegean Conference on Electrical Machines and Power Electronics, September 2007, pp. 587−591.
[28] M.G. Fakhry, A. Massoud, S. Ahmed, Quasi seven-level operation of multilevel converters with selective harmonic elimination, in: 2014 26th International Conference on Microelectronics (ICM), December 2014, pp. 216−219.
[29] J. Hao, G. Zhang, Y. Zheng, W. Hu, K. Yang, Solution for selective harmonic elimination in asymmetric multilevel inverter based on stochastic configuration network and levenberg-marquardt algorithm, in: 2019 IEEE Applied Power Electronics Conference and Exposition (APEC), March 2019, pp. 2855−2858.
[30] M. Mohaddes, A.M. Gole, P.G. McLaren, Application of an artificial neural network to harmonic reduction in PWM ac-dc converter, in: IEEE WESCANEX 95. Communications, Power, and Computing. Conference Proceedings, vol. 1, May 1995, pp. 123−128.
[31] F. Filho, H.Z. Maia, T.H.A. Mateus, B. Ozpineci, L.M. Tolbert, J.O.P. Pinto, Adaptive selective harmonic minimization based on ANNs for cascade multilevel inverters with varying dc sources, IEEE Trans. Ind. Electron. 60 (5) (May 2013) 1955−1962.
[32] Ieee Recommended Practice and Requirements for Harmonic Control in Electric Power Systems, IEEE Std 519-2014, June 2014, pp. 1−29 (Revision of IEEE Std 519-1992).
[33] F. Chollet, et al., Keras, 2015. https://keras.io.
[34] A. Moeini, S. Wang, A dc link sensor-less voltage balancing technique for cascaded h-bridge multilevel converters with asymmetric selective harmonic current mitigation-PWM, IEEE Trans. Power Electron. 33 (9) (2017) 7571−7581.